Optical and theoretical investigations of small InP quantum dots in $Ga_xIn_{1-x}P$

J. Persson* and M. Holm
Solid State Physics/The Nanometer Consortium, Lund University, P.O. Box 118, 221 00 Lund, Sweden

C. Pryor
Optical Science and Technology Center, University of Iowa, Iowa City, Iowa 52242

D. Hessman, W. Seifert, L. Samuelson, and M.-E. Pistol
Solid State Physics/The Nanometer Consortium, Lund University P.O. Box 118, 221 00 Lund, Sweden
(Received 13 February 2002; revised manuscript received 5 June 2002; published 23 January 2003)

We have studied small InP quantum dots in a GaInP matrix theoretically and experimentally. Using low-temperature photoluminescence spectroscopy in conjunction with six band $\mathbf{k}\cdot\mathbf{p}$ calculations, including direct and exchange interactions, we show that the dot size is a crucial parameter that determines whether the dot is neutral or charged with electrons in the nominally undoped *n*-type host material. For a small enough quantum dot, the conduction-band ground state is positioned above the Fermi level and the dot remains neutral. However, as soon as the dot is large enough for the conduction-band ground state to be located below the Fermi level the dot is charged. Furthermore, we show that, for neutral quantum dots, the position of the bi-exciton emission line with respect to the exciton emission line depends on the size of the quantum dot and that the bi-exciton emission can be on either side of the exciton emission: for the smallest dots the bi-exciton emission is always at higher energy than the exciton emission but for larger dots the ordering is the opposite with the exciton emission line on the high-energy side.

DOI: 10.1103/PhysRevB.67.035320 PACS number(s): 78.55.Cr, 78.67.Hc, 73.21.La

I. INTRODUCTION

Optical investigations of individual quantum dots (QD's) are becoming more and more interesting due to progress in the fabrication of low-density samples as well as in microscopy techniques. One of the most widely studied systems is quantum dots grown by the Stranski-Krastanow technique. These quantum dots are usually coherent with the barrier material and give strong photoluminescence. Investigations of individual quantum dots have shown effects of few-particle states,[1–4] strongly nonlinear electron-phonon coupling,[5] random telegraph noise,[6] and nonclassical photon statistics.[7,8] The most widely studied system is In(Ga)As dots in GaAs, but we will here concentrate on the less well studied system of InP dots in GaInP. Such dots usually grow in a bimodal fashion.[9] There are thus two sets of dots: (i) fully developed dots with a typical size of 15 nm in height and 40 nm in width, and (ii) smaller dots with a height of less than 5 nm and a width of about 40 nm. The fully developed dots have been investigated by transmission electron microscopy (TEM),[10] atomic force microscopy,[11] scanning tunnelling microscopy,[12] and scanning tunnelling induced luminescence,[13] single dot photoluminescence (PL),[14] time-resolved photoluminescence,[15] capacitance spectroscopy,[16] and by theoretical modeling both of the electronic structure[17] as well as of the equilibrium shape.[18] These dots have proven to be suitable candidates for red lasers.[19]

One of the most significant features of the fully developed InP dots is that they are highly charged in *n*-type materials and the photoluminescence is dominated by emission from charged excitons.[20] This is because the energy of the electron ground state in the dot is below the Fermi level. We will here present evidence that the small InP dots can be charged or neutral, depending on the energy of the electron ground state. We will also show that the emission of the bi-exciton can be either on the low-energy side of the exciton emission line or on the high-energy side, depending on dot size. Furthermore, we will show that experiment and theory agree well with each other.

II. EXPERIMENT

The samples were grown by metal-organic vapor-phase epitaxy at low pressure. Initially a lattice matched layer of $Ga_{0.51}In_{0.49}P$ was grown on GaAs. Subsequently, two monolayers of InP was grown, which formed quantum dots after a 12-s growth interrupt. A final cap layer of 100 nm GaInP was then grown. The sample was not rotated during the growth, resulting in a gradient in the dot density. In some regions of the samples the separation of small dots was sufficiently large that single dots could easily be measured. The samples were *n*-type with a carrier concentration of about 10^{16} cm^{-3}.

For the photoluminescence measurements, a frequency-doubled yttrium-aluminum-garnet laser emitting at 532 nm was used. The samples were mounted in a cold finger cryostat and a typical measurement temperature was 10 K. The emission was collected by a microscope, equipped with a long working distance objective having a numerical aperture of 0.4. For increased light collection efficiency we also used a 3-mm hemisphere solid immersion lens with a refractive index of 1.83.[21] The emission was usually dispersed by a single, 0.46-m, spectrometer but in some cases a double, 0.85-m, spectrometer was used. The signal was detected with a charge-coupled device camera cooled by liquid nitrogen. In order to vary the excitation power density we used neutral density filters. Integration times from a few seconds up to

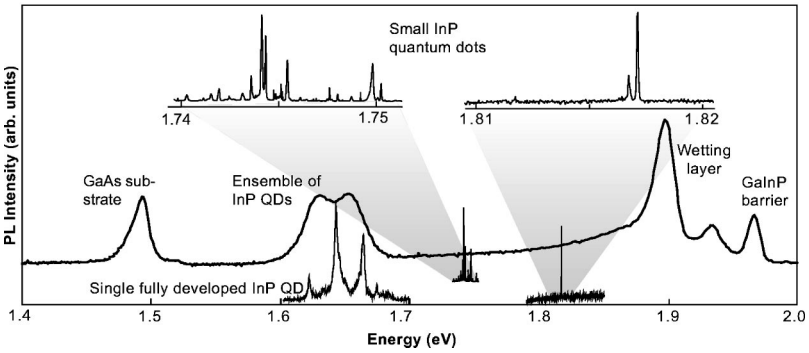

FIG. 1. The middle trace shows the macro-PL spectra of a typical sample. At an energy of about 1.65 eV there is emission from fully developed InP quantum dots having multiple, and quite broad, emission lines. This is true also for the spectrum of individual dots. At higher energy, for example 1.8 eV, there is emission from small InP quantum dots which have narrow emission lines. There is also emission from the substrate, the wetting layer, and the GaInP barrier.

several hours were used, depending on the excitation power density. About 100 dots in ten samples have been investigated with very similar results.

III. EXPERIMENTAL RESULTS

Figure 1 shows PL spectra of a typical sample. The middle trace is a macro-PL spectrum where the main emission features come from the GaAs substrate at 1.5 eV, the distribution of emission from the fully developed InP quantum dots is centered at 1.65 eV, and at 1.9 eV and above the emission is from the InP wetting layer and the GaInP barrier material. The figure also has a representative spectrum of a fully developed dot, which shows the presence of several broad emission lines distributed over basically the same range as the dot ensemble. At higher energy, between 1.65 and 1.9 eV, there is emission from the smaller quantum dots. Emission spectra from two such dots are also shown in the figure. For the smaller dots the spectra consists of emission lines which are substantially narrower than for the fully developed QD's and are limited by the spectral resolution of our detection system, 50–100 μeV, depending on configuration. This behavior is very consistent from sample to sample and essentially disproves the hypothesis that fluctuations in the charge state of the matrix are responsible for the linewidth of the fully developed dots in our samples, although a different behavior has been observed by other groups.[22] The large linewidth of fully developed InP dots has instead been attributed to a short dephasing time caused by a large number of electrons in the dot.[20] In fact, if the number of electrons is reduced, the linewidth of the fully developed dots become narrow. Such a reduction of the number of electrons in the dots was achieved by a controlled change in the Fermi level using an applied electric bias.[20] In Fig. 2(a) we show spectra of a small dot emitting at an energy of about 1.7 eV. The spectra consist of a multitude of lines, also at the lowest possible excitation power density we could use, which is very similar to the fully developed dots.

We attribute the large number of emission lines in Fig. 2(a) to emission from charged excitons in this dot. The number of lines as well as the emission energy range is consistent with this interpretation and will be further discussed in Sec. V (theoretical results). It is expected that the precise position of the Fermi level with respect to the electron ground state determines whether the dot should be charged or not. That is, if the electron ground state is positioned above the Fermi level, the dot should not be charged, indicated in the insets of Fig. 2.

We have therefore investigated dots emitting at higher energy and one example is shown in Fig. 2(b). In this case the photoluminescence spectra consist of very few lines at low excitation power density. At higher excitation power density, new emission lines appear within a few meV from the original lines. This behavior is very similar to the behavior of In(Ga)As dots in GaAs, and is attributed to formation of multiexciton complexes at higher excitation power densities.[1–3] At the lowest excitation power density we could use, the dot has a dominant emission line at 1.8128 eV, which we attribute to emission from an exciton. At higher excitation power densities, we observe emission also at 1.8123 eV, which we attribute to emission from bi-excitons. At even higher excitation power density we observe additional lines, which we attribute to tri-excitons. Our assignment of the bi-exciton is somewhat uncertain and we cannot exclude this line to be due to a charged exciton. However, different dots emitting at different energies, but being neu-

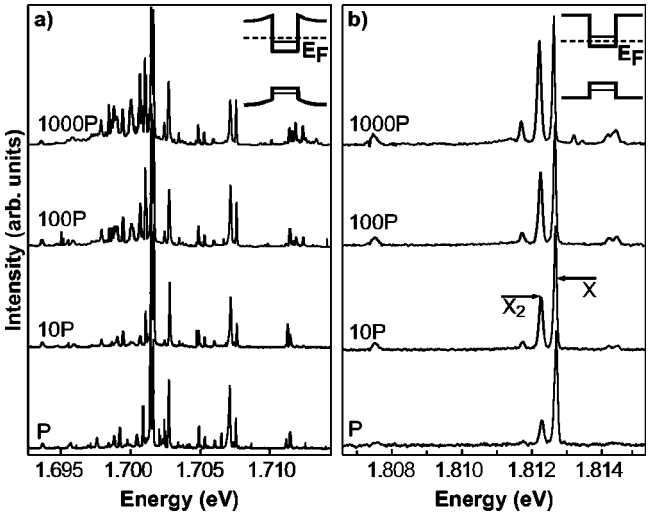

FIG. 2. Small InP quantum dots showing drastically different spectral behavior. In (a) the spectra consist of a large number of sharp lines, whereas in (b), at slightly higher energy, the spectra consist of a few lines under low excitation power density and scales highly nonlinear as the laser power is increased. We attribute the differences in the spectra from different charge situations, where the dot in (a) is charged and the dot in (b) is neutral, demonstrated in the insets.

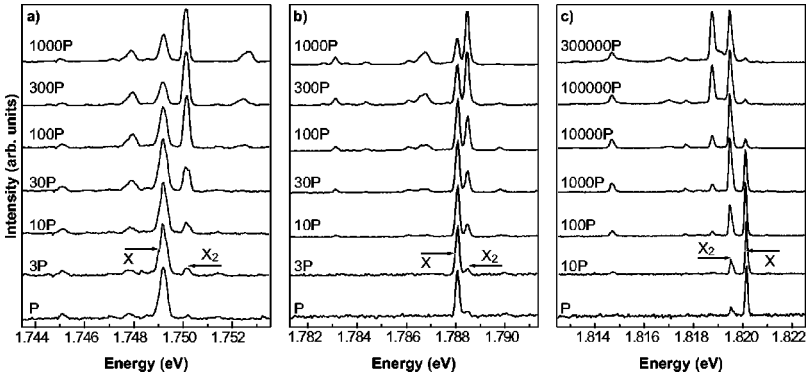

FIG. 3. Neutral dots of different size having a different relative separation of the exciton and bi-exciton lines. In (a) the dominating exciton line is at 1.749 eV while the energy of the biexciton line is approximately 1 meV higher. In (b) the distance is less than 0.4 meV and in (c) the lines have changed positions and the distance is about 0.7 meV with the bi-exciton on the low-energy side.

tral, show a very similar behavior which argues against the hypothesis that the relative position of the electron energy and the Fermi level is important (as long as the Fermi level is below the ground state of the electron). In our experiments we usually obtain a linear increase of the intensity with increasing excitation power density for the exciton emission line but a nearly quadratic increase for the biexciton. Although this is not complete evidence that our assignment is correct it is not in disagreement. The spectral boundary separating charged and neutral dots has been found to vary somewhat between samples. This is not particularly surprising since the doping concentration, and thus the Fermi-level position, varies somewhat from sample to sample. The unique shape and strain situation of the individual quantum dot will also affect the position of the spectral boundary.

One puzzling aspect of the few-particle states in InAs quantum dots in GaAs relates to the emission energy of the bi-exciton compared to the exciton emission. Most studies have shown that the bi-exciton emission occurs at a lower energy than the exciton emission,[23] but there are also studies that show the opposite ordering.[24,25] In Fig. 3 we show PL spectra of InP dots having different emission energies (but still assumed to be neutral), as a function of excitation power density. We find that for dots emitting at high energy, the bi-exciton emission is on the low-energy side of the exciton line. However, for dots emitting at lower energy the ordering is different with the bi-exciton emitting at a higher energy than the exciton.

In Fig. 4 we have plotted the experimental energy differences between the bi-exciton and the exciton emission as a function of the exciton emission energy. We have also calculated this difference and we find an essentially complete agreement between experiment and theory. Thus the ''binding energy'' of the bi-exciton can be either positive or negative for small InP quantum dots, depending on the dot size. We believe that the same situation is true for InAs quantum dots in GaAs, which would resolve the apparent contradiction in the literature. The agreement between theory and experiment lends further support to our interpretation of the emission lines as due to excitons and bi-excitons.

IV. THEORY

In order to verify the experimental results, we have made theoretical investigations of small InP quantum dots using the multiband $\mathbf{k}\cdot\mathbf{p}$ theory in the envelope function approximation. Strain effects on the electronic structure of the dot material as well as the matrix material were modeled using the finite element method and the strain-dependent Hamiltonian.[26,27] This theory has been successfully applied to fully developed InP quantum dots in GaInP,[17] and InAs quantum dots in InP.[28] The theory has also been used for calculating the energy[29,30] and optical oscillator strengths of multiexciton complexes in InAs quantum dots in GaAs.[25]

Energy levels and wave functions were calculated in a single-particle approximation by solving a strain-dependent $2+6$ band $\mathbf{k}\cdot\mathbf{p}$ Hamiltonian using the Lanczos algorithm. Relevant material parameters used in the calculations can be found in Ref. 17. In order to take account of both direct Coulomb interaction and particle-particle interactions, such as the exchange interaction, a multiparticle base was formed out of products of the single-particle wave functions. Because of Kramer's degeneracy the single-particle wave functions are twofold degenerate. We can thus form $2^{n_e+n_h}$ different basis functions, or products, given n_e and n_h single-particle electron and hole states, respectively. For example, by denoting the time-reversal operator T, we can expand the exciton (X) wave function in a linear combination of all possible combinations of products between filled orbitals according to

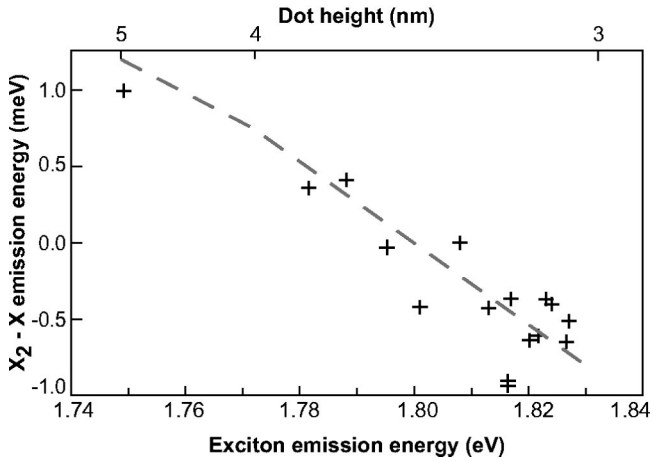

FIG. 4. Experimental and theoretical distances between exciton and bi-exciton emission. Positive values corresponds to a situation where the bi-exciton emission is at higher energy than the exciton; see Figs. 3(a) and (b). The dashed line is the calculated situation, showing excellent agreement with experiments.

$$\Psi(\vec{r}_e,\vec{r}_h)=a\varphi_e(\vec{r}_e)\varphi_h(\vec{r}_h)+b[T\varphi_e(\vec{r}_e)]\varphi_h(\vec{r}_h)+c\varphi_e(\vec{r}_e)[T\varphi_h(\vec{r}_h)]+d[T\varphi_e(\vec{r}_e)][T\varphi_h(\vec{r}_h)], \tag{1}$$

where $\varphi_e(\vec{r}_e)$ and $\varphi_h(\vec{r}_h)$ are the ground-state electron and hole single-particle orbitals and $(a-d)$ are the expansion coefficients. To solve the multiparticle Schrödinger equation by using first-order perturbation theory we need to diagonalize the $2^{n_e+n_h}$ Hamiltonian given by

$$H=H_0+H_{direct}+H_{exch}, \tag{2}$$

where H_0 is the single-particle Hamiltonian, H_{direct} and H_{exch} are the direct and exchange Coulomb interaction, respectively. Both H_0 and H_{direct} are diagonal in the basis of product functions, like $\varphi_e(\vec{r}_e)\varphi_h(\vec{r}_h)$, but H_{exch} is not. The exchange interaction represented by H_{exch} is actually divided into two pieces, one short-range and one long-range. The short-range part is from the interaction within a unit cell while the long-range part is from the interaction between different unit cells. Because the short-range piece dominates in strength we will not consider the long-range piece. The short-range piece is sometimes called the ''empirical contact interaction.'' The empirical contact interaction (eci) consists of an ''analytic'' and a ''nonanalytic'' part.[31] These parts are also sometimes called short-range and long-range interaction, which can be very confusing. The empirical contact interaction, thus representing both the analytic and the nonanalytic part, is given by

$$H_{exch,eci}=\alpha(\vec{\sigma}\cdot\vec{J}), \tag{3}$$

where α is a coupling constant, $\vec{\sigma}$ the spin-$\frac{1}{2}$ operator acting on the Γ_6 components of the conduction band, and $\vec{J}$ is the spin-$\frac{3}{2}$ operator acting on the Γ_8 components of the valence band. The form of the exchange energy operator given by Eq. (3) can be deduced by symmetry considerations.[32]

In our calculations, we have used an exchange coupling parameter α of 0.2 eV nm^3. Following the relations of Ref. 31, this value results in a reasonable exchange split of less than 0.1 meV for bulk InP.

Equation (3) is only valid for the case when we have decoupled conduction and valence bands. This does not constitute a problem because of the comparable large band gap of InP resulting in a weak coupling between electrons and holes. In order to find the energies of the different multiparticle states we have to compute the matrix elements of $H_{exch,eci}$, given by Eq. (3), in the product function basis and then perform a trivial diagonalization. Assuming a spin up electron and using Pauli two-component and four-component formalism the matrix elements of the exchange operator between an electron and a hole will be on the form

$$\langle\varphi_i(\vec{r}_e)\varphi_j(\vec{r}_h)|H_{exch,eci}|\varphi_k(\vec{r}_e)\varphi_l(\vec{r}_h)\rangle=\alpha\int d^3r_e\begin{bmatrix}F_{i1}(\vec{r}_e)\\F_{i2}(\vec{r}_e)\end{bmatrix}^{\dagger}\vec{\sigma}\begin{bmatrix}F_{k1}(\vec{r}_e)\\F_{k2}(\vec{r}_e)\end{bmatrix}\cdot\int d^3r_h\begin{bmatrix}F_{j3}(\vec{r}_h)\\F_{j4}(\vec{r}_h)\\F_{j5}(\vec{r}_h)\\F_{j6}(\vec{r}_h)\end{bmatrix}^{\dagger}\vec{J}\begin{bmatrix}F_{l3}(\vec{r}_h)\\F_{l4}(\vec{r}_h)\\F_{l5}(\vec{r}_h)\\F_{l6}(\vec{r}_h)\end{bmatrix}, \tag{4}$$

where F_{im} is the envelope function for orbital i and band index m, $\vec{\sigma}=(\sigma_x,\sigma_y,\sigma_z)$ is the angular momentum operator in the $j=1/2$ space, and $\vec{J}=(J_x,J_y,J_z)$ is the angular momentum operator in the $j=3/2$ space. By including the exchange interaction we take the spinor structure of the multiparticle state of interest into account. In a quantum dot, an originally four times degenerate state will split due to the exchange interaction and due to the low (or nonexisting) symmetry into four nondegenerate levels. These four levels occur in two closely spaced pairs where the lowest pair has a very low transition probability.

We specify the different multiparticle states by the occupation numbers of the single electron and single hole orbitals.[25] For example, in our notation the four different exciton states are denoted $(e10{:}h10)_{1-4/4}$, meaning that we have one electron and one hole in their single-particle ground states and no electrons or holes in the excited level(s). The subscript specifies the different states within an exchange-split multiplet as well as the total number of states.

In order to gain information about the transition amplitudes of recombining electron-hole pairs, we have calculated the transition matrix elements in the linear dipole approximation, assuming a transverse electromagnetic field. We keep track of the fermionic character of the particles, i.e., the antisymmetry of the wave function, in transitions by the use of electron and hole creation and annihilation operators, denoted $(a^{\dagger},b^{\dagger})$ and (a,b), respectively, obeying anticommutation relations. For example, consider the state $|e20{:}h20\rangle=a_1^{\dagger}a_2^{\dagger}b_3^{\dagger}b_4^{\dagger}|0\rangle$, where the numeric subscript indicates distinct orbitals and $|0\rangle$ is the vacuum state characterized by the condition $a|0\rangle=0$, $b|0\rangle=0$. The dipole operator can be constructed of the annihilation operators and the dipole vector operators of the different possible transitions according to $\vec{P}=\Sigma_{i,j}\vec{p}_{ij}a_ib_j$. It follows that $\langle e10{:}h10|\vec{P}|e20{:}h20\rangle=\vec{p}_{13}-\vec{p}_{14}-\vec{p}_{23}+\vec{p}_{24}$, where the minus signs indicate the antisymmetric character of the wave function.

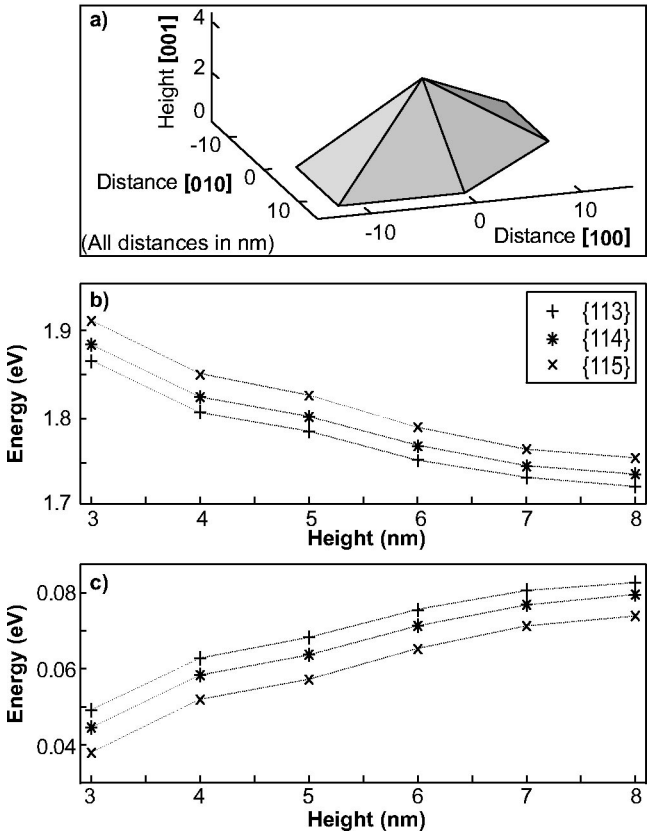

FIG. 5. (a) Geometry used for the theoretical calculations. The example given is an island of 4 nm height. The surfaces are {114}-like and the structure is based on TEM studies. (b) Ground-state energy levels in the conduction band as a function of dot height. Three different geometries, having surfaces of type {113}, {114}, and {115}, have been calculated. (c) Ground-state energy levels in the valence band as a function of dot height. The same three geometries as in (b) were used.

V. THEORETICAL RESULTS

Figure 5 shows the geometry of the InP quantum dot used in the calculations. We use a pointed pyramid with $\{10n\}$- and $\{11n\}$-type surfaces and with a height in the range 3–8 nm. The size and geometry was obtained by inspections of cross-sectional TEM images.[33]

Single-particle energy levels (ground states) are also shown in Fig. 5 as a function of dot height for three different dot geometries. The dependence on the geometry is not very pronounced and we have chosen the geometry with {114}-like surfaces for the more detailed calculations involving multiparticle states.

Figure 6 shows the level diagram of the exciton and the bi-exciton. The exciton is split into four levels: two dark almost degenerate levels and two, optically allowed, excited levels with a splitting of about 0.3 meV situated 5 meV above the dark states. We believe that this split, although the line is forbidden, sometimes is observable as a line on the low-energy side of the main exciton emission line, as in Fig. 3(a) at 1.745 eV. The direct interaction contributes to a binding energy of the exciton of about 20 meV.

Although the exchange splitting in bulk is small, it can be much larger in a quantum dot due to the confinement.[31] Several publications report considerably smaller splits. For example, Bayer *et al.* measures an exchange split of 0.15 meV for InGaAs dots in GaAs.[34] However, experiments on colloidal InAs (Ref. 35) and InP (Ref. 36) quantum dots, as well as epitaxially grown CdSe/ZnSe (Ref. 37) and InAs/GaAs (Ref. 25) dots, report values of several meV. The explanation to these discrepancies could merely be a manifestation of the $1/R^3$ dependence of the exchange splitting,[31] making it very sensitive to the size of the quantum dots. The $1/R^3$ dependence of the exchange splitting is derived for dots having infinitely high confining barriers and is weaker for dots with finite barriers, e.g., Stranski-Krastanow grown quantum dots. The effect of size should thus be stronger for colloidal dots with a very strong localization of the charges. However, an inspection of our calculated wave functions shows that both electrons and holes are strongly localized inside the dots despite having finite barriers.

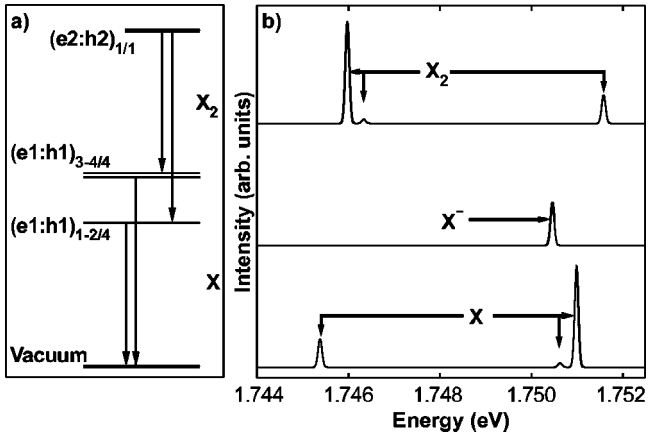

FIG. 6. (a) shows the states involved in the decay chain of the bi-exciton. (b) demonstrates calculated spectra with emission from the exciton X, the charged exciton X^-, and the bi-exciton X_2. In the figure, the emission from the dark states have been enhanced for visibility.

In Fig. 6(b) we can see a simulated spectrum of a recombining exciton (X), a charged exciton (X^-) and a bi-exciton (X_2) for a 4-nm dot. The symmetric arrangement of the exciton and the bi-exciton lines, with respect to energy, can be easily understood by inspection of the level diagram presented in Fig. 6(a). The equal transition amplitudes are caused by the symmetry between the initial state in the bi-exciton recombination, $(e20{:}h20)_{1/1}$, and the final state in the exciton recombination, $(e00{:}h00)_{1/1}$, i.e., the vacuum state. A charged exciton contributes only with one single, twofold degenerated line. The calculated transition amplitudes cannot be directly compared to the intensities seen in PL, since the experimental intensities are highly dependent on the occupation probability of the various possible initial states, and can also be influenced by phonon interaction.

In Fig. 4 we have plotted the transition energies of the bi-exciton relative to the transition energy of the exciton, as a function of the quantum dot height. There is a very good agreement between theory and experiment. Figure 7 shows a simulated spectrum of a doubly charged exciton (X^{2-}) and

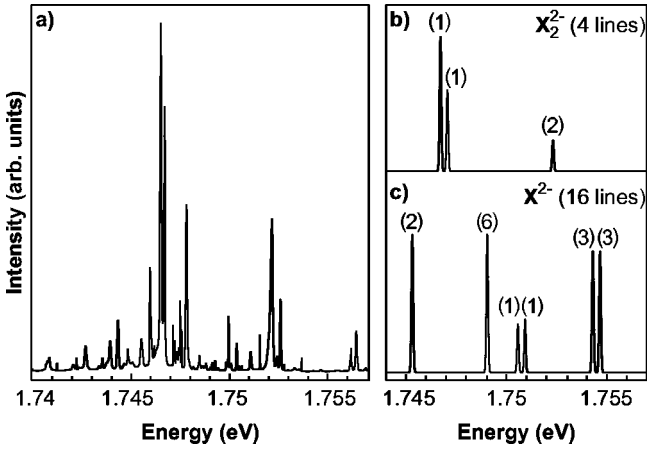

FIG. 7. Experimental (a) and simulated (b) spectra of a doubly charged exciton (X^{2-}) and bi-exciton (X_2^{2-}) involving transitions of the type $(e21{:}h10) \rightarrow (e11{:}h00)$, 16 lines, and $(e22{:}h20) \rightarrow (e12{:}h10)$, 4 lines.

of a doubly charged bi-exciton (X_2^{2-}) involving transitions of the type $(e21{:}h10) \rightarrow (e11{:}h00)$ and $(e22{:}h20) \rightarrow (e12{:}h10)$, respectively. The charged exciton X^{2-} contributes theoretically with 16 different lines while the charged bi-exciton X_2^{2-} has only four possible transitions when no excited electron orbitals are involved. The degeneracy of the levels are indicated in the figure and is to a large extent due to the C_{2v} symmetry of the dot. The dots that we measure most likely do not have any remaining symmetry. The number of emission lines from a doubly charged exciton then agrees quite well with the observed number of lines. Thus it is likely that we observe the X^{2-} emission for dots emitting at a low energy. There are, however, more lines in the experimental spectra than in the computed one. It is unclear why this is the case but it appears that we also observe transitions involving excited hole states. Such a situation has previously been found in InAs QDs in GaAs.[38] It is clear that a large amount of research is needed to give a complete and reliable assignment of every peak of a spectrum such as that in Fig. 7(a).

VI. CONCLUSIONS

In conclusion we have shown that the size of a quantum dot, or more specifically the electron ground-state energy of the dot relative to the Fermi level, is a very crucial parameter that determines whether a dot is charged or remains neutral in a weakly doped host material. An electron ground state located below the Fermi level allows the dot to be charged whereas it stays neutral if the ground state is higher than the Fermi-level, i.e., for a small enough quantum dot. We have also shown that the doubly charged dot heavily complicates the emission spectrum, and that our calculations, in terms of number of lines and emission energy range, agrees rather well with the experimental data presented.

In addition, we have shown that the bi-exciton emission energy with respect to the exciton emission energy is size dependent and can be on either side of the exciton emission energy. For dots small enough, the main exciton peak is always positioned on the high-energy side of the biexciton but for slightly larger dots, the ordering is opposite.

ACKNOWLEDGMENTS

This work was performed within the Nanometer Consortium in Lund and was supported by the Swedish Research Council (VR), and the Swedish Foundation for Strategic Research (SSF).

*Electronic address: jonas.persson@ftf.lth.se

[1] L. Landin, M. S. Miller, M.-E. Pistol, C. E. Pryor, and L. Samuelson, Science **280**, 262 (1998).

[2] E. Dekel, D. Gershoni, E. Ehrenfreund, D. Spektor, J. M. Garcia, and P. M. Petroff, Phys. Rev. Lett. **80**, 4991 (1998).

[3] M. Bayer, O. Stern, P. Hawrylak, S. Fafard, and A. Forchel, Nature (London) **405**, 923 (2000).

[4] K. Hinzer, P. Hawrylak, M. Korkusinski, S. Fafard, M. Bayer, O. Stern, A. Gorbunov, and A. Forchel, Phys. Rev. B **63**, 075314 (2001).

[5] A. Zrenner, M. Markmann, E. Beham, F. Findeis, G. Böhm, and G. Abstreiter, J. Electron. Mater. **28**, 542 (1998).

[6] M.-E. Pistol, P. Castrillo, D. Hessman, J. A. Prieto, and L. Samuelson, Phys. Rev. B **59**, 10 725 (1999).

[7] C. Santori, M. Pelton, G. Solomon, Y. Dale, and Y. Yamamoto, Phys. Rev. Lett. **86**, 1502 (2001).

[8] V. Zwiller, H. Blom, P. Jonsson, N. Panev, S. Jeppesen, T. Tsegaye, E. Goobar, M.-E. Pistol, L. Samuelson, and G. Björk, Appl. Phys. Lett. **78**, 2476 (2001).

[9] N. Carlsson, W. Seifert, A. Peterson, P. Castrillo, M.-E. Pistol, and L. Samuelson, Appl. Phys. Lett. **65**, 3093 (1994).

[10] K. Georgsson, N. Carlsson, L. Samuelson, W. Seifert, and L. R. Wallenberg, Appl. Phys. Lett. **67**, 2981 (1995).

[11] M.-E. Pistol, J.-O. Bovin, A. Carlsson, N. Carlsson, P. Castrillo, K. Georgsson, D. Hessman, T. Junno, L. Montelius, C. Persson, L. Samuelson, W. Seifert, and L. R. Wallenberg, *Proceedings of the 23rd International Conference on the Physics of Semiconductors*, edited by M. Scheffler and R. Zimmermann (World Scientific, Singapore, 1996), p. 1317.

[12] P. Ballet, J. B. Smathers, H. Yang, C. L. Workman, and G. J. Salamo, Appl. Phys. Lett. **77**, 3406 (2000).

[13] U. Håkanson, M. K.-J. Johansson, J. Persson, J. Johansson, M.-E. Pistol, L. Montelius, and L. Samuelson, Appl. Phys. Lett. **80**, 494 (2002).

[14] D. Hessman, P. Castrillo, M.-E. Pistol, C. Pryor, and L. Samuelson, Appl. Phys. Lett. **69**, 749 (1996).

[15] V. Zwiller, M.-E. Pistol, D. Hessman, R. Cederström, W. Seifert, and L. Samuelson, Phys. Rev. B **59**, 5021 (1999).

[16] S. Anand, N. Carlsson, M.-E. Pistol, L. Samuelson, and W. Seifert, Appl. Phys. Lett. **67**, 3016 (1995).

[17] C. Pryor, M.-E. Pistol, and L. Samuelson, Phys. Rev. B **56**, 10 404 (1997).

[18] Q. K. K. Liu, N. Moll, M. Scheffler, and E. Pehlke, Phys. Rev. B **60**, 17 008 (1999).

[19] Q. M. K. Zundel, N. Y. Jin-Phillipp, G. Phillipp, K. Eberl, T. Riedl, E. Fehrenbacher, and A. Hangleiter, Appl. Phys. Lett. **73**, 1784 (1998).
[20] D. Hessman, J. Persson, M.-E. Pistol, C. Pryor, and L. Samuelson, Phys. Rev. B **64**, 233308 (2001).
[21] W. L. Barnes, G. Björk, J. M. Gerard, P. Jonsson, J. A. E. Wasey, P. T. Worthing, and V. Zwiller, Eur. Phys. J. D **18**, 197 (2002).
[22] P. G. Blome, M. Wenderoth, M. Hubner, R. G. Ulbrich, J. Porsche, and F. Scholz, Phys. Rev. B **61**, 8382 (2000).
[23] E. Dekel, D. Gershoni, E. Ehrenfreund, J. M. Garcia, and P. M. Petroff, Phys. Rev. B **61**, 11 009 (2000).
[24] E. Moreau, I. Robert, L. Manin, V. Thierry-Mieg, J. M. Gerard, and I. Abram, Phys. Rev. Lett. **87**, 183601 (2001).
[25] L. Landin, M.-E. Pistol, C. Pryor, M. Persson, L. Samuelson, and M. Miller, Phys. Rev. B **60**, 16 640 (1999).
[26] T. B. Bahder, Phys. Rev. B **41**, 11 992 (1990).
[27] T. B. Bahder, Phys. Rev. B **45**, 1629 (1992).
[28] M. Holm, M.-E. Pistol, and C. Pryor, J. Appl. Phys. **92**, 932 (2002).
[29] C. Pryor, Phys. Rev. B **57**, 7190 (1998).
[30] C. Pryor, Phys. Rev. B **60**, 2869 (1999).
[31] S. V. Goupalov and E. L. Ivchenko, J. Cryst. Growth **184/185**, 393 (1998).
[32] G. L. Bir and G. E. Pikus, *Symmetry and Strain-Induced Effects in Semiconductors* (Wiley, New York, 1975).
[33] W. Seifert, N. Carlsson, M. Miller, M.-E. Pistol, L. Samuelson, and L. R. Wallenberg, Prog. Cryst. Growth Charact. Mater. **33**, 423 (1996).
[34] M. Bayer, O. Stern, A. Kuther, and A. Forchel, Phys. Rev. B **61**, 7273 (2000).
[35] U. Banin, J. C. Lee, A. A. Guzelian, A. V. Kadavanich, and A. P. Alivisatos, Superlattices Microstruct. **22**, 559 (1997).
[36] O. I. Micic, H. M. Cheong, H. Fu, A. Zunger, J. R. Sprague, A. Mascarenhas, and A. J. Nozik, J. Phys. Chem. B **101**, 4904 (1997).
[37] J. Puls, M. Rabe, H.-J. Wunsche, and F. Henneberger, Phys. Rev. B **60**, R16 303 (1999).
[38] M. Persson, N. Panev, L. Landin, S. Jeppesen, and M.-E. Pistol, Phys. Rev. B **64**, 075309 (2001).